An Observational Study of Medium-Scale Wave Dynamics in the Southern Hemisphere Summer. Part II: Stationary–Transient Wave Interference

WILLIAM J. RANDEL AND JOHN L. STANFORD

Physics Department, Iowa State University, Ames, IA 50010

(Manuscript received 17 September 1984, in final form 15 February 1985)

ABSTRACT

Eastward moving, baroclinically forced, medium-scale waves are frequently observed to dominate the Southern Hemisphere summer circulation. In addition, strong quasi-stationary medium-scale waves were also observed during the summer of 1978/79. In this paper we present the results of an observational study for several weeks of this time period, during which the stationary and transient waves are found to exhibit clear linear interference characteristics. Energetic analyses indicate that the medium-scale waves grow barotropically and decay baroclinically during this period, although these interference induced contributions are secondary to the usual baroclinic growth-barotropic decay life cycle characteristics observed by Randel and Stanford. Data analyses and simple model calculations are presented which demonstrate that the observed baroclinic decay results from equatorward heat flux associated with the differing vertical structures of the stationary and transient waves. An interference induced feedback mechanism between the medium-scale waves and the zonal-mean flow is discussed.

1. Introduction

Several recent studies have demonstrated that the Southern Hemisphere (SH) summer atmosphere is frequently dominated by eastward moving, medium-scale (zonal wavenumbers 4–7) waves (Salby, 1982; Hamilton, 1983; Randel and Stanford, 1983; Yu *et al.* 1983). In a companion paper (Randel and Stanford, 1985a; hereafter RS1), the dynamics of these medium-scale waves were studied for three SH summers. It was found that the SH summertime flow vacillates between periods of medium-scale wave domination and relatively quiet, zonally symmetric states. The medium-scale waves result from baroclinic instabilities, and exhibit a clearly defined life cycle of baroclinic growth, maturity, and barotropic decay. A particular case study of such a life cycle is detailed in Randel and Stanford (1985b), and the results are found to be in excellent agreement with modeled medium-scale baroclinic waves (Simmons and Hoskins, 1978).

In addition to the eastward propagating, baroclinically forced, medium-scale waves, quasi-stationary medium-scale waves were also observed during the summer of 1978/79 (Kalnay and Paegle, 1983; Randel and Stanford, 1983). Randel and Stanford (1983) observed a clear correlation between the medium-scale wave energy and the phase of transient wave 5 during this summer, suggestive of stationary-transient wave interference. Eliassen–Palm flux diagrams during a particular growth and decay episode clearly demonstrated that the waves were interacting barotropically with the mean flow, and commensurate mean-flow kinetic energy changes were observed. Energetic studies (discussed in RS1) have since confirmed that the medium-scale waves indeed grow barotropically during these interference episodes, although the dominant forcing mechanism is still baroclinic.

This paper reports further analyses of the stationary-transient interference characteristics, particularly a study of the interference induced medium-scale wave heat flux. This analysis is motivated by observations of *equatorward* heat flux and baroclinic *decay* associated with the time period studied here, although at no other time during the three summers studied in RS1. We demonstrate here that the interference of the stationary and transient medium-scale waves results in an induced heat flux, harmonically varying with the period of the transient wave. Estimates of this heat flux based on the observed wave structure are in good agreement with observed values. This agreement provides confirmation of the interference hypothesis, and suggests an interference induced feedback mechanism which may have helped maintain the medium-scale waves during this summer.

Linear wave interference between zonal wavenumber 1 traveling and stationary waves in the Northern Hemisphere winter atmosphere has been well documented by Madden (1975, 1983). He has demonstrated that the alternating constructive and destructive interference results in harmonic variations in the zonally averaged heat and momentum budgets, along with the zonal mean wind and temperature fields. This present work provides another example of linear wave interference in a somewhat different setting,

again emphasizing the resulting fluctuations in large-scale circulation.

2. Structure of the stationary medium-scale wave

Large-amplitude stationary medium-scale Rossby waves in the SH summer of 1978/79 were first noted in results from a global analysis using Global Weather Experiment observations (Kalnay-Rivas *et al.*, 1981; Kalnay and Halem, 1981). Further observational properties were noted in Kalnay and Paegle (1983) and Randel and Stanford (1983). A summary of the stationary wave characteristics is discussed here.

A problem arises when attempting to isolate the structure of these stationary waves, because they are not truly constant in time. The nodes and antinodes remain fixed in space, while their amplitude changes (over a much longer time scale than that associated with the transient waves). This feature is suggestive of stationary Rossby wave dispersion, and distinguishes these stationary waves from truly climatological mean waves in the SH summer, which have been shown to be of planetary scale (k = 1–3) and much weaker than those in the NH (van Loon and Jenne, 1972; Trenberth, 1980). An additional complication arises because the stationary waves discussed here have approximately the same horizontal scale as the baroclinically forced traveling waves discussed in RS1, and their interaction complicates attempts of isolating either one.

An estimate of the stationary wave structure is made here by the time average over two complete periods of the transient wave. Figure 1 displays the 200 mb geopotential height contours averaged over the 28-day period, 24 December 1978–20 January 1979. The choice of this time period is based on the energetic analyses to be discussed in Section 3.

Zonally asymmetric wave patterns with typical horizontal wavelengths of 50–70° longitude (zonal wavenumbers k = 5–7) are observed in Fig. 1, with maximum amplitude close to 30–40°S near South America. Little vertical phase tilt is observed; the waves exhibit an equivalent barotropic structure peaking near 200 mb. Possible origins of these stationary waves are discussed in Randel (1984) and Kalnay and Mo (1984). Note that such strong stationary waves are not evident during February 1979.

It is interesting to note that the horizontal scales of these SH quasi-stationary waves are similar to those of zonally oriented wave trains observed in the Northern Hemisphere with time scales on the order of 10–30 days, whose characteristics are also suggestive of Rossby wave dispersion (Blackmon *et al.*, 1984).

3. Identification of stationary-transient wave interference

Although medium-scale wave amplitude vacillations occur during each summer studied in RS1, these

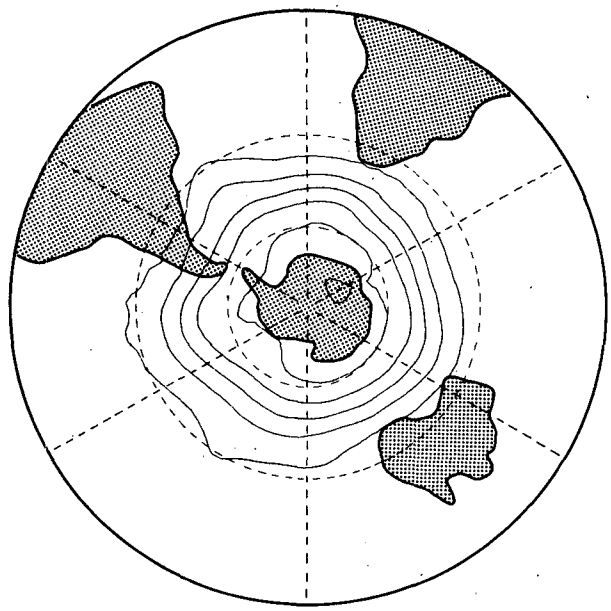

FIG. 1. Polar stereographic projection of the time-averaged 200 mb geopotential height contours for the period 24 December 1978–20 January 1979. Contour interval is 200 gpm. Note the zonally-asymmetric wave patterns on the scale of zonal wavenumber 5, with largest amplitudes near South America.

vacillations occur much more regularly during 1978/79. In addition, the medium-scale wave amplitude is found to be correlated with the wave phase during this summer. Figure 2 shows this correlation: the medium-scale wave energy is plotted at the bottom, along with the phase of transient wave 5 at the top. Wave amplitude maxima are observed each time the transient wave phase is in a particular position; i.e., within the shaded region. This correlation can also be clearly observed in hemispheric geopotential height charts; inspection of Figs. 8a–d of RS1 clearly shows that the medium-scale waves are amplified when in phase with the time-mean structure seen in Fig. 1. This correlation between wave amplitude and phase suggests a) stationary-transient wave interference, and/or b) preferred region(s) of wave amplification (for example, a localized highly baroclinic region that enhances baroclinic wave growth).

To distinguish between these possible mechanisms, the medium-scale wave energetics are studied to determine the cause of the wave growth. These energetic calculations are detailed in Appendix B of RS1. While the amplitude-phase correlation (Fig. 2) is apparent throughout the 1978/79 summer, close study of the energetics during this year (Fig. 10a of RS1) reveals that during the first several weeks of January 1979, there are some additions to the "usual" baroclinic-growth barotropic-decay scheme observed repeatedly during each summer in RS1.

Figure 3 details the energetics of waves 5–7 during this period: the waves are observed to *grow barotrop-*

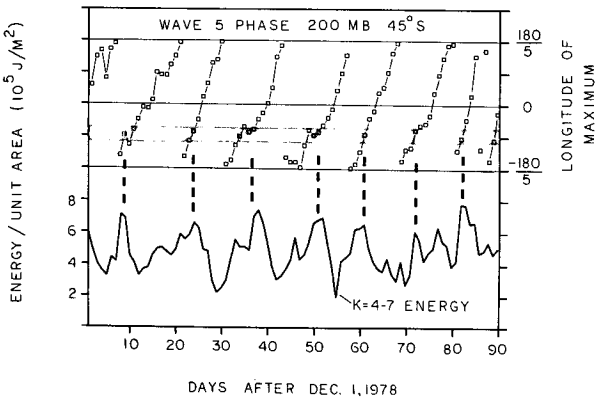

FIG. 2. Top: Phase of wave 5 at 45°S latitude and 200 mb during 1978–79. Bottom: Medium-scale wave energy during 1978–79. Note that wave energy maxima are observed each time the phase of wave 5 is near the shaded region. [Adapted from Randel and Stanford (1983)]

ically on days 32–33 and 48–49 and *decay baroclinically* on days 27–28 and 39–41. We view these additions to the "usual" energy cycle as indications of some additional dynamical processes occurring over this time period. Moreover, the presence of the stationary waves during this time clearly points to an interference-based mechanism. The distinguishing energetics observed during these several weeks are consistent with the time varying nature of the stationary medium-scale waves discussed in Section 2. The stationary waves apparently achieve their largest amplitude during this time, and thus exhibit the clearest interference characteristics with the transient waves. Note that baroclinic growth is still the dominant mechanism for wave amplification; this indicates that the transient waves are undergoing their "usual" energy cycle while at the same time interacting with the stationary wave (which may in turn modify the "usual" growth-decay scheme).

Eliassen–Palm (EP) flux diagrams provide details of the wave structure and mean flow interaction during these growth and decay periods. Figure 9a of Randel and Stanford (1983) showed an EP flux diagram for wave 5 during the barotropic growth period (day 32 of Fig. 3 here). It was shown that this barotropic wave growth is accompanied by a divergence of wave momentum flux in the mid-to-upper troposphere in midlatitudes, centered near 45°S. A decrease in the zonal-mean jet was observed, along with a decrease in the zonal-mean kinetic energy commensurate with this wave growth (Fig. 8 of Randel and Stanford, 1983). A decrease in the zonal wind speed causes an apparent slowing down (with respect to an observer on the surface of the earth) of the wave imbedded in the flow; this is in agreement with the slower phase progression of wave 5 observed in the top of Fig. 2 near days 35 and 50.

The EP cross section shown in Fig. 9b of Randel and Stanford (1983) during decay of the wave (day 40 in Fig. 2 here) shows strong barotropic decay, and, in addition, *equatorward* heat flux over the region 45–55°S and 400–850 mb. This equatorward heat flux is associated with the baroclinic decay observed on day 40 of Fig. 3. Figure 4 shows the medium-scale wave poleward heat flux during this summer of 1978–79, averaged over 40–50°S in the lower troposphere (700–850 mb), along with the medium-scale wave energy for reference. Equatorward heat transport is observed in Fig. 4 near days 30 and 40, coincident with the time period studied here, although at no other time during the season. A simple model of interfering waves (to be introduced in Section 4) will demonstrate that such equatorward heat flux may, under certain circumstances, result from linear wave interference.

4. Modeled interference induced heat flux

a. Simple interference model

A simple analytical model of interfering transient and stationary waves is presented here to help understand this interaction. Although this is a grossly simplified model, it demonstrates important features that can result from interference. It will be shown that the observed medium-scale wave heat flux can be partially understood in terms of this model.

This latitude-independent model is based on the linear superposition of one purely transient wave and one purely stationary wave, both of the same zonal wavenumber k. Each wave has amplitude varying in

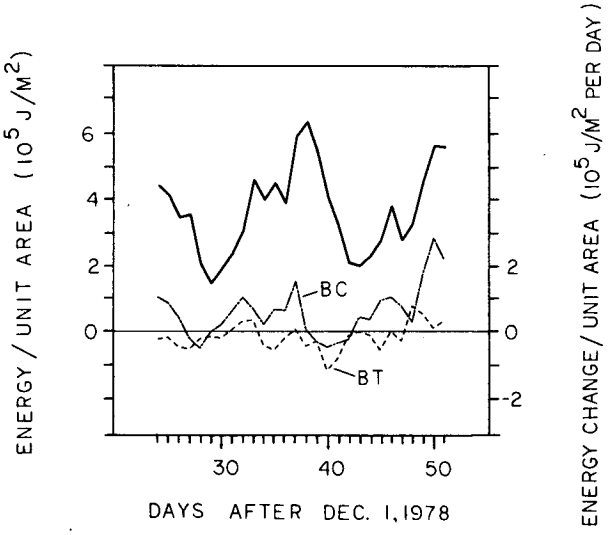

FIG. 3. Detail of energetics of waves 5–7 during 1978/79 interference episode. Heavy solid line is wave energy, plotted along with changes due to baroclinic (BC) and barotropic (BT) wave-mean flow interactions. Note barotropic growth near days 33 and 48 and baroclinic decay near days 28 and 40.

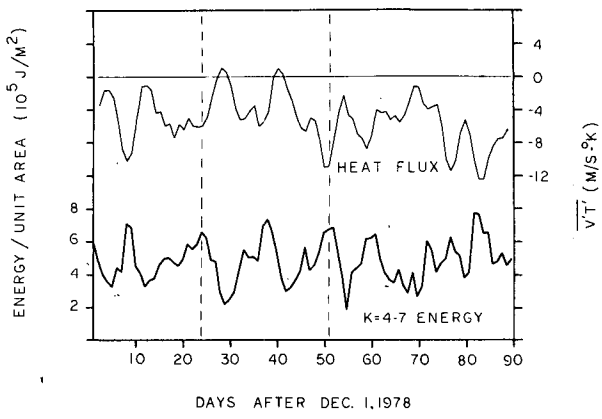

FIG. 4. Time variations in medium-scale wave heat flux, averaged over 40–50°S and 700–850 mb, along with the medium-scale wave energy (heavy solid line) for reference. A 1-1-1 moving filter has been applied to the heat flux time series for smoothing. Negative values denote transport towards the South Pole. Dashed vertical lines indicate the time period covered in Fig. 2. Note the equatorward heat transport observed near days 30 and 40.

the vertical but constant phase tilts with height. The geopotential height perturbations for each are given by

$$\Phi_T(\lambda, z, t) = A_T(z) \sin(k\lambda + m_T z - \sigma t) \quad \text{(transient)},$$

$$\Phi_S(\lambda, z) = A_S(z) \sin(k\lambda + m_S z) \quad \text{(stationary)},$$

where T and S refer to transient and stationary quantities, respectively. The vertical wavenumbers m_T and m_S will be chosen such that the resulting sine function has variations that are slow in the vertical; the vertical amplitude dependence is intended to be predominantly contained in the functions $A_T(z)$ and $A_S(z)$. Evaluating the resulting velocity perturbations geostrophically, and the temperature fluctuations hydrostatically, we may write the zonally-averaged heat flux resulting from these waves as

$$\overline{v'T'}(t) = \left(\frac{g^2 Hk}{2Rfr\cos\theta}\right)\Big\{\underbrace{m_T A_T^2 + m_S A_S^2}_{\text{A}} + \underbrace{[m_T + m_S]A_T A_S \cos[(m_S - m_T)z + \sigma t]}_{\text{B}} - \underbrace{[A_S \partial A_T/\partial z - A_T \partial A_S/\partial z] \sin[(m_S - m_T)z + \sigma t]}_{\text{C}}\Big\}. \quad (1)$$

Here g is the gravitational acceleration, H the scale height, R the gas constant, f the Coriolis parameter, r the earth's radius, and θ latitude (negative in the SH).

The terms A, B, and C in Eq. (1) result from different physical processes. Term A represents the (time-independent) heat flux due to each wave individually. Term B results from the direct overlap of the stationary and transient waves. It varies harmonically in time with the period $2\pi/\sigma$ of the transient wave, maximizing when the waves are in phase. Term C depends on differing vertical amplitude structures for the two waves; if the waves are identical [$A_T(z) = A_S(z)$], no interaction occurs. This term also varies harmonically in time with the period $2\pi/\sigma$ of the transient wave, although it maximizes when the two waves are one-quarter cycle *out of phase*. Note that if both waves tilt westward with height, terms A + B will always combine to give a net poleward heat flux, whereas term C suggests that *equatorward* heat flux can result from the interference of these waves.

b. *Application of model*

In this section an estimate of the interference induced heat flux will be made based on variations

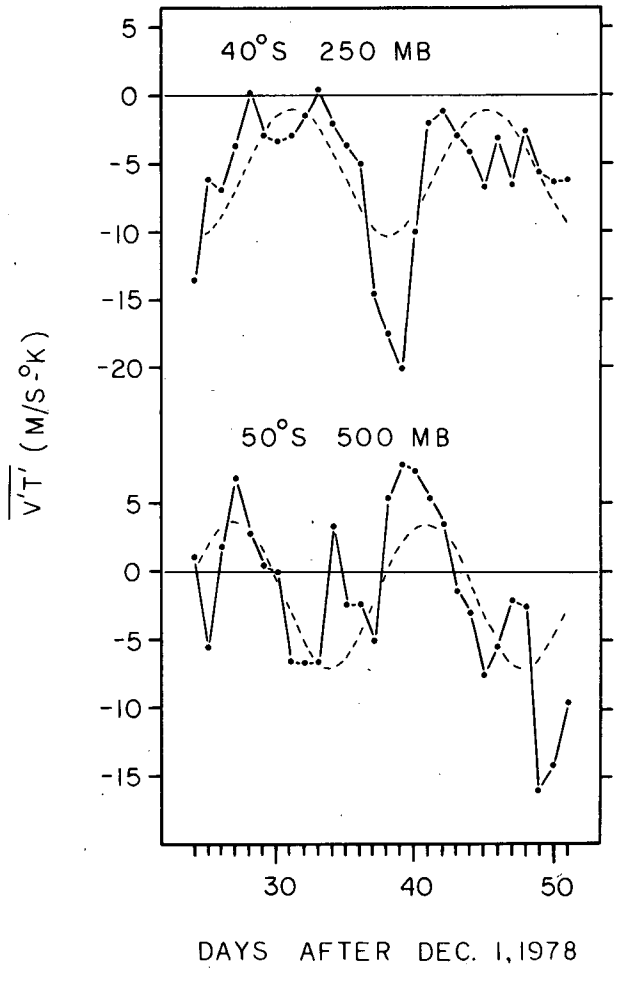

FIG. 5. Zonally averaged northward heat flux for each day during two cycles of stationary-transient wave interference. Top: 40°S latitude, 250 mb. Bottom: 50°S latitude, 500 mb. Individual values are given by the dots, while the second harmonic of each series is shown by the dashed line.

in the observed total heat flux. This result will then be compared to that estimated from the simplified model, using the observed stationary and transient wave structures incorporated into Eq. (1). The results are in modest agreement, and suggest that interference is the cause of the observed *equatorward* heat flux during decay of the interfering waves.

The observed heat flux will be studied for the time interval shown in Fig. 3 (i.e., between days 24 and 51 of 1978/79), during which approximately two complete interference cycles are observed. Each interference episode thus lasts approximately 14 days. The interference model Eq. (1) predicts a harmonically dependent interference-induced heat flux. The actual heat fluxes at 40°S, 250 mb and 50°S, 500 mb are shown in the top and bottom, respectively, of Fig. 5, along with the second harmonic of the time series for each. The second harmonic, which accounts for approximately 40% of the variance at each of these positions, will be used as an estimate of the interference induced contribution to the total heat flux. Note that much of the heat flux variations throughout the troposphere are probably associated with the "usual" baroclinic growth processes observed in Fig. 3; the

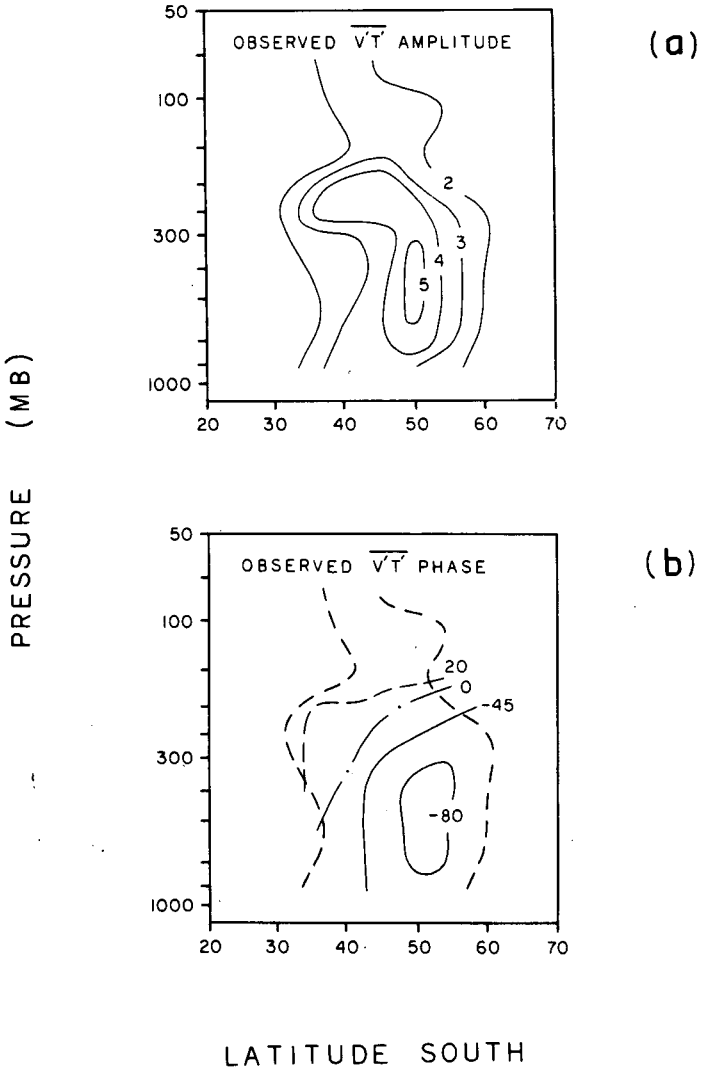

FIG. 6. Meridional cross sections of the observed amplitude (a) and phase (b) of the interference-induced heat flux. Estimates are made by using the second harmonic of the heat flux time series at each latitude and pressure, as in Fig. 5. Units in (a) are (m s^{-1}-°K), while the phase (time of maximum *poleward* heat flux) in (b) is in degrees. The phase is measured such that zero refers to the two waves constructively interfering. A value of −90 degrees thus refers to maximum poleward heat flux occurring one quarter cycle before the transient wave phase reaches that of the stationary wave.

two locations in Fig. 5 have been chosen so as to display the maximum interference induced contributions. Similar harmonic analyses at each latitude (25–65°S) and pressure (850–50 mb) result in meridional cross sections of the amplitude and phase (in time) of the interference induced heat flux. These are shown in Fig. 6a, b. The phase (time of the maximum *poleward* heat flux) is measured such that zero refers to the two waves constructively interfering.

Close inspection of the amplitude and phase plots reveals two separate areas where the observed heat flux is "coherent" in time: 1) 35–40°S, 200–300 mb and 2) 45–55°S, 300–850 mb. By "coherent," we mean regions of slowly varying heat flux phase, with significant amplitude. The phase diagram (Fig. 6b) indicates that the upper-level (200–300 mb) maximum poleward heat flux occurs when the stationary and transient waves are nearly in phase, while the lower-level (300–850 mb) maximum occurs when the transient wave *lags* the stationary wave by approximately one-quarter cycle. The center of these two areas are out of phase by approximately 110 degrees (0.31 cycle, or 4.3 days), consistent with the phase difference between the dashed curves in Fig. 5.

To apply Eq. (1) to the observed wave structure, estimates must be made for the vertical wavenumbers m_T and m_S (assumed here to be constant over the entire period). As shown in the baroclinic wave case study of Randel and Stanford (1985b), the vertical slope of the transient wave changes in time; here we want only a rough estimate. This is done by applying term A from Eq. (1), i.e., relating the observed time-averaged heat flux to the time-averaged transient and stationary waves over this period. From this rough estimate, $m_T + m_S$ is found to be approximately $0.3/H$, where H is the atmospheric scale height (approximately 7 km).

An estimate of the stationary wave amplitude is made by time averaging the geopotential coefficients over the 28 day period. The transient wave's amplitude is estimated by subtracting the stationary wave's coefficients from each day's values, and then time-averaging the resulting wave amplitudes. Figure 7a shows the resulting stationary wave amplitude (A_S), while Fig. 7b shows that for the transient wave (A_T). It is important to note the differing meridional cross sections for these waves; their differing vertical structures suggest their possible interaction through term C of Eq. (1). Figure 7c shows the overlap term ($A_S A_T$), while Fig. 7d shows the vertical difference term

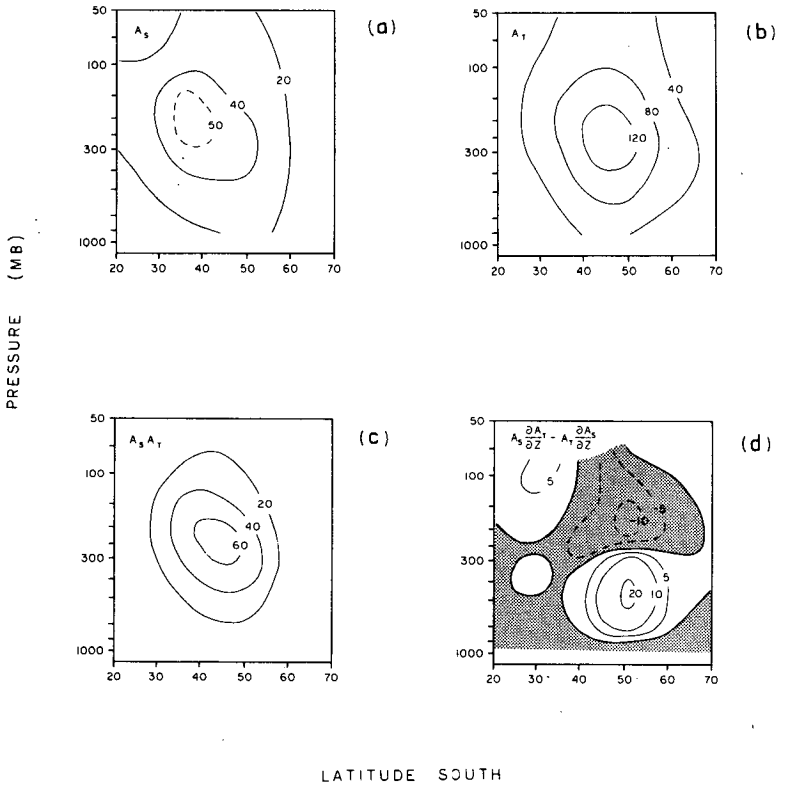

FIG. 7. Meridional cross sections of average stationary (S) and transient (T) wave structure over interference episode. (a) stationary wave amplitude (gpm); (b) transient wave amplitude (gpm); (c) stationary-transient overlap (OV term in text—10^2 gpm^2); (d) vertical difference (MD term in text—10^2 gpm^2 H^{-1}).

$(A_S\partial A_T/\partial z - A_T\partial A_S/\partial z)$. The amplitude and phase of the modeled heat flux are given by [using Eq. (1), with $m_T = m_S = m$]:

$$\text{amplitude} = \left(\frac{g^2Hk}{2RFr\cos\theta}\right)(\text{OV}^2 + \text{MD}^2)^{1/2}$$

$$\text{phase} = \tan^{-1}(\text{OV/MD}),$$

where

$$\text{OV} = (2m)(A_SA_T),$$

is the overlap term, and

$$\text{MD} = -(A_S\partial A_T/\partial z - A_T\partial A_S/\partial z)$$

is the vertical difference term.

Such calculations at each latitude and pressure (based on the observed wave structures seen in Fig. 7) result in the modeled heat flux amplitude and phase cross sections shown in Fig. 8a, b. The model structure is seen to be similar to the observed cross sections (Fig. 6a, b). The modeled amplitude structure hints at double maxima: near 50°S in the midtroposphere (400–500 mb), and near 40–45°S in the upper troposphere (200–250 mb). The phase structure (Fig. 8b) further delineates the two areas, as each is roughly coherent (in time). The estimated phases are close to the observed values, and the phase difference between these two "coherent" regions is predicted to be approximately 100 degrees, close to the observed value.

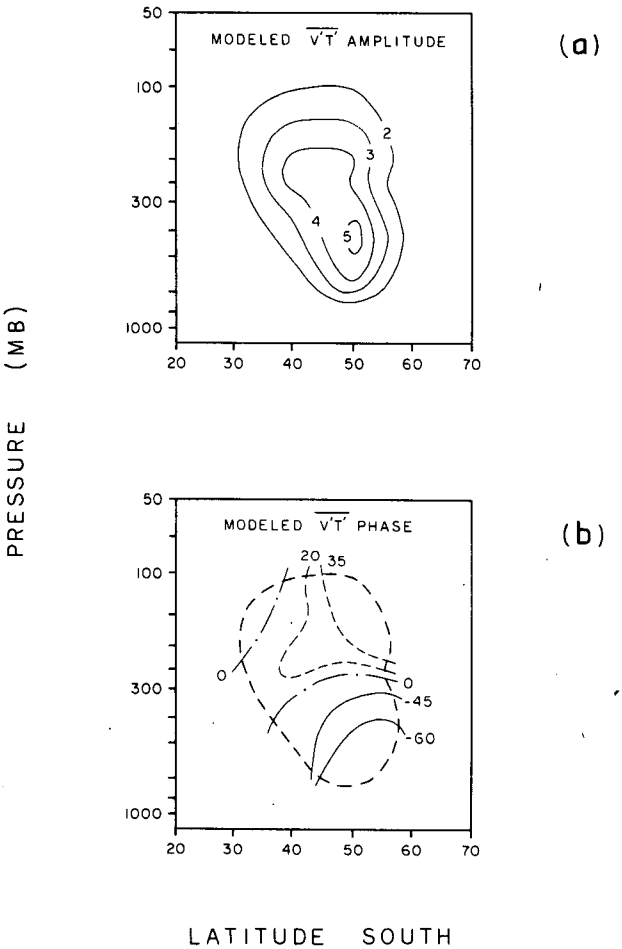

FIG. 8. As in Fig. 6, but for (a) modeled heat flux amplitude and (b) phase, based on simple interference model calculations. Fig. 6 gives the observed distributions.

This agreement allows the underlying physics of this part of the interference interaction to be understood in terms of the simple model. The upper tropospheric heat flux maximum is the result of the direct overlap of heat flux from each wave separately, reaching a maximum when the waves are in phase. No equatorward heat flux results, only a modulation of the amount of poleward flux. This analysis is in agreement with the observed values in the top of Fig. 5.

The lower heat flux maximum is a result of the differing vertical structures of the transient and stationary waves. This is shown schematically in Fig. 9. When the transient wave lags the stationary wave by one-quarter cycle, the stationary waves' advection of the transient wave's temperature perturbation ($v'_ST'_T$, proportional to $A_S\partial A_T/\partial z$) is larger than the transient wave's advection of the stationary wave's temperature perturbation ($v'_TT'_S$, proportional to $A_T\partial A_S/\partial z$). The average of $(A_S\partial A_T/\partial z - A_T\partial A_S/\partial z)$ over a complete wavelength is thus positive. Half a cycle later, when the transient wave leads the stationary wave by one-quarter cycle, the situation is reversed, and the net heat flux is *equatorward.* This analysis is also in good agreement with the observed values in the bottom of Fig. 5: the modeled results are thus consistent with the interference hypothesis.

The data and simple model results describe how the interference of traveling and stationary waves causes a harmonically dependent heat flux, which would not otherwise occur. The phase of this interaction is such that poleward heat flux is enhanced prior to the stationary-transient wave overlap, while equatorward heat flux is produced as the waves move out of phase. This equatorward heat flux results in a baroclinic decay period observed in Fig. 3. Note that this interaction is entirely dependent on the relative vertical structures of the two waves, and different dynamics can be expected in other circumstances. It is apparently fortuitous that in this case the induced baroclinic decay occurs so as to enhance the decay already occurring. In addition, these results suggest that baroclinic growth may be enhanced (or initiated) by this mechanism.

The baroclinic decay observed here results in an increase of the zonal mean temperature gradient, or baroclinicity, of the zonal mean flow. This flow is then more conducive to the growth of baroclinically unstable waves: the transient waves will grow (perhaps initiated by the poleward heat flux associated with the beginning of the next interference cycle), and

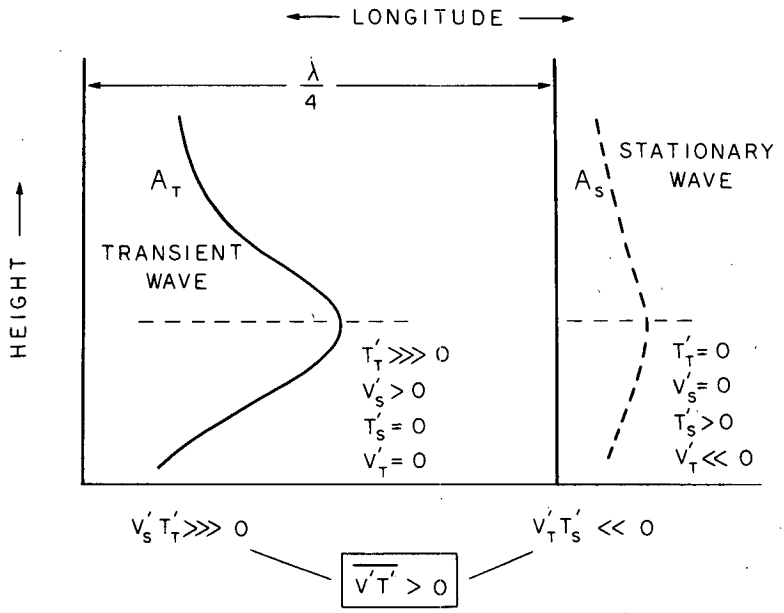

FIG. 9. Schematic illustration of differing vertical structures of stationary and transient waves, and resulting net wave heat flux. This heat flux is maximized when the two waves (of the same zonal scale) are one-quarter cycle out of phase, as indicated in the top of the figure. Perturbation velocities and temperatures associated with each wave are indicated, and their relative sizes indicated by the number of "greater than" signs for each.

interfere again with the stationary wave. This feedback mechanism may account for the regular occurrence of the wave 5 structures during the summer of 1978/79. (Note that only waves of the same zonal scale as the stationary wave—approximately wave 5 in 1978/79—will contribute to this mechanism.) The important ingredient (and major difference from the other summers studied in RS1) is the presence of the stationary medium-scale wave during the Global Weather Experiment year.

Attempts to use a similar model to understand the momentum fluxes associated with interference were generally unsuccessful. This is perhaps due to the fact that a model with constant latitudinal phase tilts is a poor approximation, compared to the assumption of constant vertical phase structure. A theoretical understanding of the interference-induced barotropic interactions thus awaits explanation.

5. Conclusion

During January 1979, stationary medium-scale waves were observed in low to middle latitudes of the SH, exhibiting characteristics suggestive of stationary Rossby wave dispersion. In addition, eastward moving baroclinically forced medium-scale waves were also observed throughout the midlatitudes. The stationary and transient waves exhibit clear interference characteristics, including 1) correlation of wave amplitude and phase, 2) barotropic wave growth, and 3) baroclinic wave decay. Our analyses demonstrate that the differing stationary and transient wave structures are responsible for the observed equatorward heat flux and baroclinic decay, and by analogy, enhanced baroclinic growth. This feedback mechanism may help account for the regular occurrence (and spectral purity) of zonal wavenumber 5 structures during the summer of 1978/79.

It is important to note that the interference induced effects detailed here are secondary to the baroclinic life cycle characteristics observed during each summer detailed in RS1. In addition, the characteristics discussed here are most apparent over only two periods of the transient wave during the summer of 1978/79, whereas the amplitude-phase correlation is evident over the entire summer (see Fig. 2). Energetic analyses (see Fig. 10a of RS1) indicate that baroclinic growth is the dominant excitation mechanism for each repeated cycle of wave growth; it is unclear whether this regularly occurring baroclinic growth is the result of localized highly baroclinic regions (related to the stationary wave), the interference induced heat flux discussed here, or a different mechanism. In any case, our results are mainly aimed at clearly identifying linear wave interference and some of its consequences in the atmosphere.

It is interesting to note that quasi-periodic fluctuations in wave intensity with a period near 20 days were noted in the SH by Webster and Keller (1975). Hamilton (1983) noted that the amplitude of wave 5

frequently varied over the same time scale as its period during the SH summers of 1972–79. One may speculate that a similar wave interference mechanism underlies these observations, although periodic wave growth is also observed in laboratory annulus experiments with no standing waves present (Pfeffer *et al.*, 1974).

Acknowledgments. This paper is based on work submitted in partial fulfillment of the requirements for the degree of Doctor of Philosophy in the Department of Physics, Iowa State University. The geopotential data were generously supplied by Mel Gelman of the Climate Analysis Center, National Oceanic and Atmospheric Administration. Support for this work has been funded by the National Science Foundation under Grant ATM 79-11879; the National Science Foundation, the National Oceanic and Atmospheric Administration, and the National Aeronautics and Space Administration under Grant ATM 81-21952; and the National Science Foundation and the National Aeronautics and Space Administration under Grant ATM 84-02901. William J. Randel has been supported by the L. H. Brown Trust Fellowship. The authors appreciate helpful discussions with Dr. Mark Schoeberl.

REFERENCES

Blackmon, M. L., Y.-H. Lee and J. M. Wallace, 1984: Horizontal structure of 500 mb height fluctuations with long, intermediate and short time scales. *J. Atmos. Sci.*, **41,** 961–979.

Hamilton, K., 1983: Aspects of wave behavior in the mid and upper troposphere of the Southern Hemisphere. *Atmos. Ocean,* **21,** 40–54.

Kalnay, E., and M. Halem, 1981: Large amplitude stationary Rossby waves in the Southern Hemisphere. *Int. Conf. Early Results of FGGE and Large Scale Aspects of its Monsoon Experiments,* Tallahassee, WMO, 3-5 to 3-15.

Kalnay-Rivas, E., W. Baker, M. Halem, R. Atlas and D. Edelmann, 1981: GLAS experiments with FGGE II-b data. *Proc. Int. Conf. Preliminary FGGE Data Analysis and Results,* Bergen, WMO, 150–161.

Kalnay, E., and J. Paegle, 1983: Large amplitude stationary Rossby waves in the Southern Hemisphere: observations and theory. *First Int. Conf. on Southern Hemisphere Meteorology,* July 31–August 6, 1983, Brazil. Amer. Meteor. Soc., Boston, 89–92.

——, and K. C. Mo, 1984: Mechanistic experiments to determine the origin of Southern Hemisphere stationary waves. *J. Atmos. Sci.*

Madden, R. A., 1975: Oscillations in the winter stratosphere: Part 2. The role of horizontal heat transports and the interaction of transient and stationary planetary waves. *Mon. Wea. Rev.,* **103,** 717–729.

——, 1983: The effect of the interference of traveling and stationary waves on time variations of the large-scale circulation. *J. Atmos. Sci.,* **40,** 1110–1125.

Pfeffer, R., G. Buzyna and W. W. Fowlis, 1974: Synoptic features and energetics of wave-amplitude vacillation in a rotating, differentially heated fluid. *J. Atmos. Sci.,* **31,** 622–645.

Randel, W. J., 1984: Structure and energetics of medium-scale atmospheric waves in the Southern Hemisphere summer. Ph.D. dissertation, Iowa State University, 171 pp.

——, and J. L. Stanford, 1983: Structure of medium-scale atmospheric waves in the Southern Hemisphere summer. *J. Atmos. Sci.,* **40,** 2312–2318.

——, and ——, 1985a: An observational study of medium-scale waves in the Southern Hemisphere summer. Part I: wave structure and energetics. *J. Atmos. Sci.,* **42,** 1172–1188.

——, and ——, 1985b: The observed life-cycle of a baroclinic instability. *J. Atmos. Sci.,* **42** (in press).

Salby, M. L., 1982: A ubiquitous wave 5 anomaly in the Southern Hemisphere during FGGE. *Mon. Wea. Rev.,* **110,** 1712–1720.

Simmons, A. J., and B. J. Hoskins, 1978: The life cycles of some non-linear baroclinic waves. *J. Atmos. Sci.,* **35,** 414–432.

Trenberth, K. E., 1980: Planetary waves at 500 mb in the Southern Hemisphere. *Mon. Wea. Rev.,* **108,** 1378–1389.

van Loon, H., and R. L. Jenne, 1972: The zonal harmonic standing waves in the Southern Hemisphere. *J. Geophys. Res.,* **77,** 992–1003.

Webster, P. J., and J. L. Keller, 1975: Atmospheric vacillations and index cycles. *J. Atmos. Sci.,* **32,** 1283–1300.

Yu, W. B., R. L. Martin and J. L. Stanford, 1983: Long and medium-scale waves in the lower stratosphere from satellite-derived microwave measurements. *J. Geophys. Res.,* **88,** 8505–8511.